Organic Electronics 137 (2025) 107180

Contents lists available at ScienceDirect

Organic Electronics

journal homepage: www.elsevier.com/locate/orgel

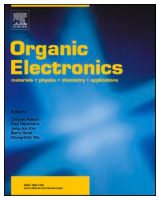

Mitigating slow reverse ISC rates in TAPC:PBD exciplex via rapid Förster energy transfer to TTPA

Lucy A. Weatherill [a], Ross Milverton [a], Piotr Pander [b,c], Fernando B. Dias [a,*]

[a] Department of Physics, Durham University, South Road, Durham, DH1 3LE, UK
[b] Faculty of Chemistry, Silesian University of Technology, M. Strzody 9, 44-100, Gliwice, Poland
[c] Centre for Organic and Nanohybrid Electronics, Silesian University of Technology, Konarskiego 22B, 44-100, Gliwice, Poland

ARTICLE INFO

Keywords:
TADF
Hyperfluorescence
FRET
OLED

ABSTRACT

There have been many advances in the development of thermally activated delayed fluorescence (TADF) materials for organic light emitting diode (OLED) applications in recent years. In particular, intramolecular exciplex systems have been highly studied and found to produce OLED devices of high external quantum efficiency (EQE) due to triplet harvesting via TADF. The proposed next generation of OLEDs uses hyperfluorescence to overcome the problem of broad emission associated with exciplexes. This process involves Förster resonance energy transfer (FRET) from the TADF host to a fluorescent dopant. In this work we revisited the photophysics of the **TAPC:PBD** exciplex (formed between the electron donor di-[4-(*N*,*N*-di-*p*-tolyl-amino)-phenyl]cyclohexane (**TAPC**) and the electron acceptor, 2-(4-biphenyl)-5-(4-*tert*-butylphenyl)-1,3,4-oxadiazole (**PBD**)) as a host capable of simultaneously performing triplet harvesting and work as a donor transferring energy to a bright fluorescent emitter. The aim is to investigate the interplay between energy transfer and intersystem crossing in this hyperfluorescence system. Contrarily to previous findings, films of the **TAPC**:**PBD** blend show relatively slow reverse intersystem crossing rate (RISC) and weak luminescence efficiency (PLQY). Despite this, when doped with the strong fluorescent emitter **TTPA**, the luminescence quantum yield is greatly improved due to the highly efficient energy transfer rate from **TAPC**:**PBD** to **TTPA**. The rapid FRET from the exciplex to the fluorescent emitter overcomes the non-radiative losses affecting the luminescence efficiency of the blend. This study shows that the hyperfluorescence mechanism not only allows colour purity in OLEDs to be optimised, but also facilitates suppressing major loss mechanisms affecting luminescence efficiency, thus creating conditions to maximizing EQE.

1. Introduction

Thermally activated delayed fluorescence (TADF) emitters are very popular in OLEDs, as they allow potentially replacing phosphorescent heavy metal complexes conventionally used to achieve high external quantum efficiencies (EQEs) [1,2]. TADF results from the up-conversion of triplet states to the first excited singlet state *via* reverse intersystem crossing (RISC). The process requires thermal energy to overcome the energy barrier for RISC [3]. Therefore, for efficient TADF to occur, the energy gap between the singlet and triplet states must be minimised. This is usually achieved by reducing the overlap between the highest occupied molecular orbital (HOMO) and the lowest unoccupied molecular orbital (LUMO) [4,5], by designing molecules where electron donor (D) and electron acceptor (A) units are covalently attached to each other or simply mixed in a solid film forming an excited state complex called an exciplex [6,7].

Exciplexes are shown to display efficient triplet harvesting due to the charge transfer nature of their excited state. The electron and hole reside on two different molecules giving minimal frontier molecular orbital overlap. This has made exciplexes attractive candidates for the emissive components of organic light emitting diode (OLED) devices [8]. In standard fluorescence OLEDs, the internal quantum efficiency (IQE) is limited to 25 % due to the formation of 75 % dark triplet states. However, OLEDs comprising exciplexes in the emissive layer can harvest light from the triplet states and hence an IQE of 100 % is theoretically possible [9]. Exciplexes also contribute for a more balanced charge distribution in the device due to their ambipolar charge transport properties.

* Corresponding author.
E-mail address: f.m.b.dias@durham.ac.uk (F.B. Dias).

https://doi.org/10.1016/j.orgel.2024.107180
Received 1 July 2024; Received in revised form 16 September 2024; Accepted 29 November 2024
Available online 30 November 2024

The drawback of exciplexes for solid state lighting is their broadband emission spectrum, and often low PLQY due to the charge transfer nature of their excited state. This gives devices of poor colour purity, and low EQE. The long luminescence lifetime – common feature of TADF materials, including exciplexes, may also promote quenching of electroluminescence due to likely interaction with charges, thus contributing to device efficiency roll-off often observed at high current densities [10,11]. Using fluorescent emitters as energy transfer acceptors from exciplexes has been proposed to solve these issues, in a mechanism that is commonly referred to as hyperfluorescence [12].

Several hyperfluorescence systems have been studied recently, with OLEDs achieving external quantum efficiency over 40 %, or up to 20–30 % without outcoupling enhancement. In these blends, the host performs the triplet-harvesting task, and transfers energy from their singlet state to a fluorescence dopant with narrowband emission spectrum and high PLQY. The dopant is kept at low concentration to minimize the occurrence of Dexter energy transfer from the host to the emitter, which will compete with triplet harvesting [13–15].

Despite, the great interest on hyperfluorescence blends in recent years, still doubts persist about some aspects of the mechanism and how it can be optimised. In this study, we investigate how the interplay between the RISC and energy transfer rates may influence the overall luminescence efficiency of the hyperfluorescence blend. For this study, a fluorescent molecule, 9,10-bis[*N*,*N*-di-(*p*-tolyl)-amino]anthracene (**TTPA**), is doped into the di-[4-(*N*,*N*-di-*p*-tolyl-amino)-phenyl]cyclohexane:2-(4-biphenyl)-5-(4-*tert*-butylphenyl)-1,3,4-oxadiazole (**TAPC:PBD)** exciplex host, see Fig. 1. This particular exciplex was chosen because of its emission spectrum that excellently matches with **TTPA** absorption, thus ensuring efficient energy transfer. The **TAPC:PBD:TTPA** blend has been previously studied by Du et al. [16], focusing on the study of two-photon excitation for bioimaging applications. They observed a strong increase on PLQY when the **TAPC:PBD** host is doped with **TTPA**, varying from 14 % in the exciplex to 98 % when **TTPA** is added. However, some of the kinetic parameters determined in their study seem unrealistically high. The reported reverse intersystem crossing (RISC) rate in the **TAPC:PBD** exciplex, $k_{RISC} = 1.91 \times 10^7\ s^{-1}$, is among the highest ever observed, presenting an intriguing anomaly. This prompted us to revisit the photophysics of this hyperfluorescence system to investigate the underlying causes of such an exceptionally high RISC rate in detail.

TTPA has an optical energy gap well-aligned with the energy of the **TAPC:PBD** exciplex, *i.e.*, the absorption spectrum of **TTPA** overlaps almost perfectly with the emission of the exciplex. **TTPA** also has a high extinction coefficient in the lowest energy absorption band and very high PLQY. Therefore, this system is ideal to probe the triplet harvesting properties of the exciplex in more detail, including an accurate investigation of the delayed fluorescence in the microsecond region under vacuum conditions. We then study the photophysics of the **TAPC:PBD** exciplex with the addition of **TTPA** dopant.

Fig. 1 shows the molecular structures of the materials involved in this study. **TAPC** is used as the electron donor, **PBD** as the electron acceptor and **TTPA** is employed as a fluorescent dopant. The energies of the HOMO and LUMO are given on the energy level diagram. These values were obtained from literature sources [17–19].

2. Results and discussion

2.1. Characterisation of the TAPC:PBD exciplex

The extinction coefficients of the exciplex components **TAPC** and **PBD** were measured in dichloromethane solution (using concentrations in the range 0.04–6.4 μM) to be $\varepsilon = (0.17 \pm 0.05) \times 10^6$ and $\varepsilon = (4.99 \pm 0.03) \times 10^6\ M^{-1}\ cm^{-1}$, respectively for **TAPC** and **PBD**, both at 305 nm. The extinction coefficients of **TAPC** and **PBD** as a function of wavelength are given in Fig. 2a) and Fig. 2b), respectively. Since the absorption spectra of the donor and acceptor are overlapping, excitation of the blend with a wavelength in the range 250–350 nm is expected to excite both components. This is true, but since **PBD** has an extinction coefficient of approximately 30 times that of **TAPC**, **PBD** is 30 times more likely than **TAPC** to be excited and promoted to the first excited singlet state under optical excitation. Therefore, we can conclude that the first step in exciplex formation is most likely to be excitation of **PBD**.

Fig. 3 shows the absorption and emission of the exciplex individual components, measured in 1 % w/w Zeonex films; plus the emission of the **TAPC:PBD** exciplex measured in neat 1:1 w/w film. The films were made by spin coating with a thickness of ~100 nm.

The exciplex absorption has been shown previously to be a simple superposition of the **TAPC** and **PBD** absorption spectra, showing that no dimers are formed in the ground state. As expected, the exciplex emission appears red shifted compared to the emission of the individual exciplex components as the exciplex state is lower in energy than the excited states of **TAPC** and **PBD**. Importantly, the exciplex emission does not contain any contribution from **TAPC** or **PBD** emission, showing that exciplex formation is very efficient [20].

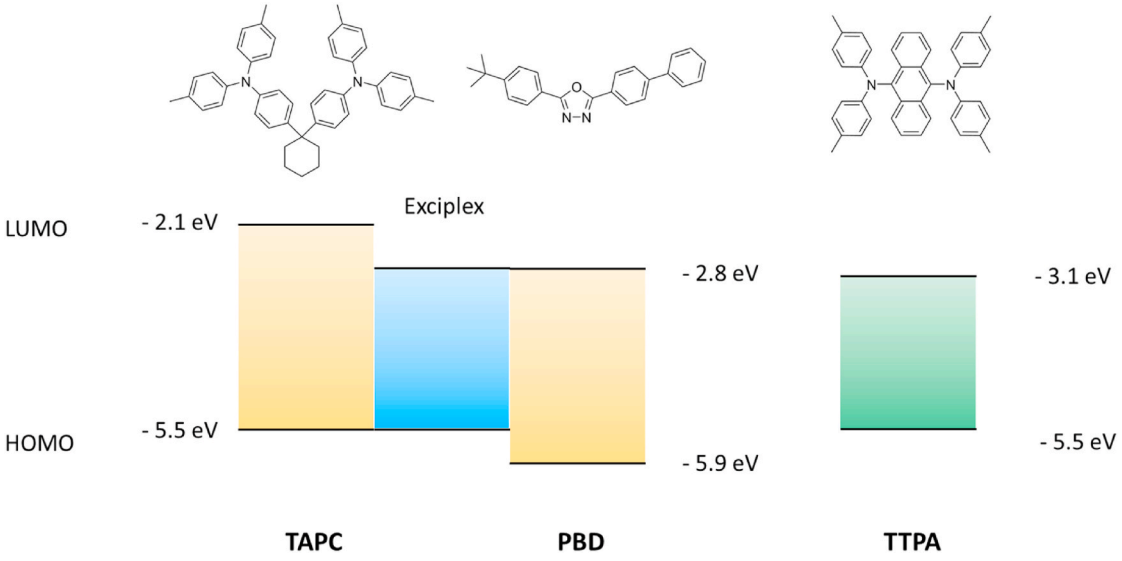

Fig. 1. Molecular structures and energy level diagram of the HOMO and LUMO of the electron donor (**TAPC**), acceptor (**PBD**) and the fluorescent dopant (**TTPA**) used in this work.

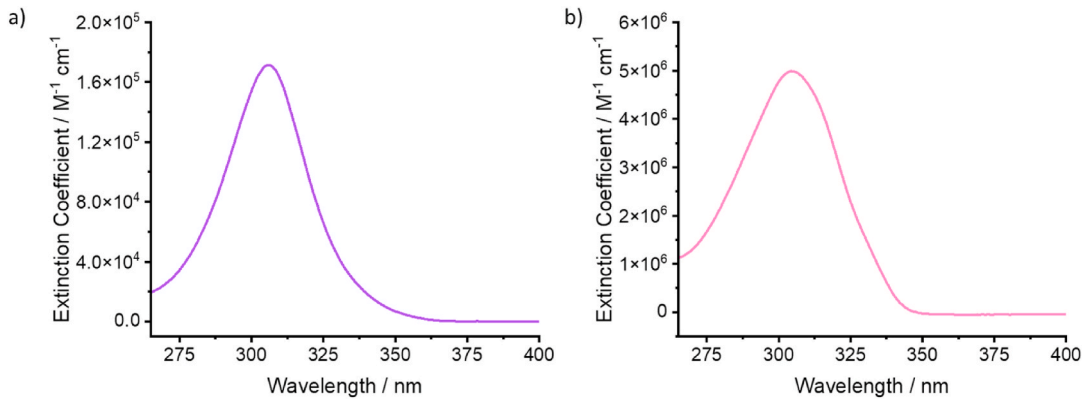

Fig. 2. Extinction coefficient as a function of wavelength for a) **TAPC** and b) **PBD**.

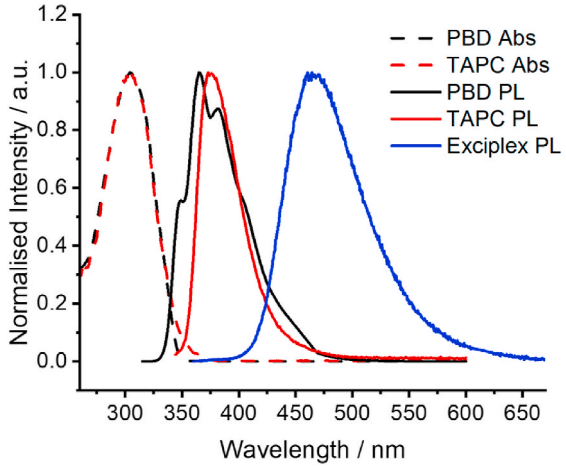

Fig. 3. Absorption (abs) and steady state emission (PL) spectra of **TAPC** and **PBD**, obtained in spin coated 1 % Zeonex films. Steady state emission (PL) spectra of the exciplex **TAPC:PBD** 1:1 neat spin coated film, $\lambda_{ex} = 305$ nm.

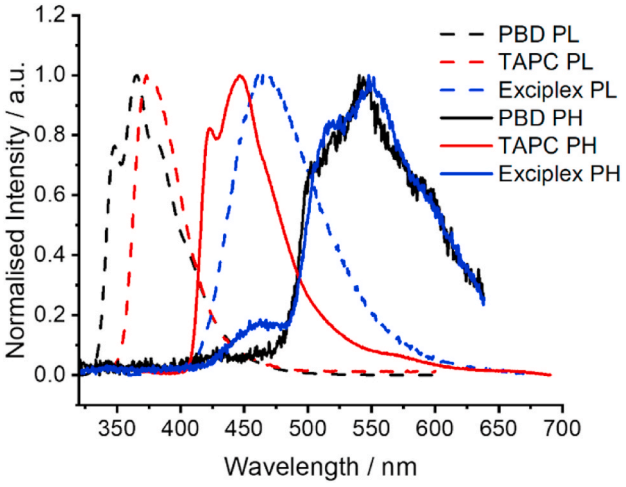

Fig. 4. Phosphorescence (PH) spectra of **PBD** and **TAPC** dispersed in Zeonex, and the phosphorescence of the **TAPC:PBD** 1:1 exciplex, all measured at 80K. The PH spectra were obtained using a delay time of 1 ms and an integration time of 50 ms. The peak at 450 nm in the exciplex PH spectrum is likely due to triplet-triplet annihilation (TTA). The steady state photoluminescence of individual **TAPC**, **PBD** and the **TAPC:PBD** 1:1 exciplex measured at room temperature are shown for reference. All films were made by drop casting.

The PLQYs of **TAPC**, **PBD** and the **TAPC:PBD** 1:1 film were measured in air with 305 nm excitation. The values obtained were 0.94, 0.06 and 0.12, respectively. The low PLQYs of **PBD** and the exciplex are likely due to efficient internal conversion in **PBD**. **PBD** is problematic because it tends to crystalise in solid neat films, and the crystal phase displays different, poor luminescent properties compared to the fresh amorphous phase. Hence, the PLQY values for **PBD** (and **TAPC** for consistency) are measured for films of 1 % **PBD** dispersed in a Zeonex host. The films were made by drop casting with an approximate thickness of 1 μm.

The phosphorescence spectra of the exciplex components measured at low temperature are given in Fig. 4 along with the steady state emission spectra at room temperature. The energies of the different states involved in the **TAPC:PBD** exciplex blend are obtained from the onset of the steady state fluorescence and phosphorescence spectra and are given in Table 1. Importantly, the phosphorescence spectrum of the exciplex clearly resembles that of **PBD**, showing the lowest triplet state is localised on this molecule (*i.e.* the **TAPC** triplet is localised at higher energy).

The almost perfect alignment between the triplet state of **TAPC** (3.03 eV) and the singlet state of the exciplex (2.98 eV) could explain the very high RISC rate reported previously. However, this has been ruled out as it is the triplet state of **PBD** that is populated. Therefore, the large $\Delta E_{ST} = 0.33$ eV is not compatible with the very high RISC rate reported previously.

The time resolved photoluminescence (TRPL) decay of the exciplex measured under vacuum is given in Fig. 5a). The lifetimes of prompt fluorescence and delayed fluorescence are calculated to be τ_{PF}, = 65.5 ns and τ_{DF} = 12.9 μs, respectively. These values were obtained from a weighted average of lifetimes from a multiexponential fit of the decay curves. The components and percentage contributions used to fit the PF and DF decay curves are given in Table 2. The observation of multi-exponential decays in solid films is often reported and attributed to the presence of molecules in different environments or adopting slightly different conformations, caused by intermolecular interactions with neighbouring molecules in the film that prevent the emitter to fully relax their excited state geometry. In such conditions different luminescence decay components are likely to be observed. In the case of D-A molecules or exciplexes, these effects are even more prevalent as the existence of different molecular orientations or environments may also affect the ISC

Table 1
Singlet and triplet energy levels for the donor, acceptor and exciplex measured in thin films.

	E_{S_1}/eV	E_{T_1}/eV	ΔE_{ST}/eV
PBD	3.52 ± 0.06	2.65 ± 0.12	0.87 ± 0.13
TAPC	3.40 ± 0.07	3.03 ± 0.04	0.37 ± 0.08
Exciplex	2.98 ± 0.02	2.60 ± 0.11	0.33 ± 0.11

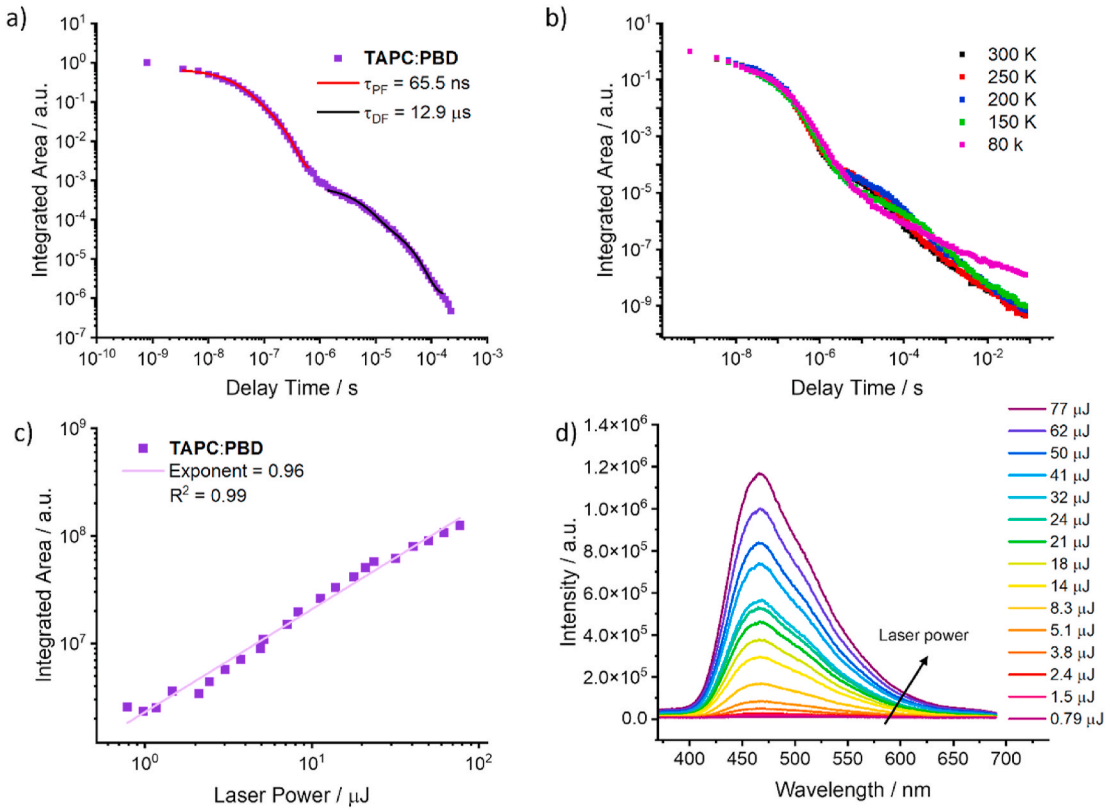

Fig. 5. Time resolved photoluminescence (TRPL) characteristics of the **TAPC:PBD** exciplex. (a) Time resolved decay measured at room temperature using 355 nm excitation from which the lifetimes of PF and DF are obtained. (b) TRPL decay as a function of temperature obtained using 355 nm excitation. (c) Intensity of delayed fluorescence as a function of excitation dose at 337 nm using a delay time of 1 µs and an integration time of 100 µs. (d) Individual delayed fluorescence spectra as a function of excitation dose (337 nm) again obtained using a delay time of 1 µs and an integration time of 100 µs.

Table 2
Components of the lifetimes used in the multiexponential fit of the decay curves in Fig. 5a). The contribution from each lifetime is given in brackets.

	Lifetime 1	Lifetime 2
Prompt fluorescence	27 ± 2 ns (0.79)	104 ± 4 ns (0.21)
Delayed fluorescence	4.1 ± 0.2 µs (0.87)	23.5 ± 0.8 µs (0.13)

and RISC rates, leading to a distribution of decay times. Fig. 5b) shows the TRPL decay as a function of temperature. This shows that the amount of DF decreases with temperature, which is consistent with the TADF mechanism due to the thermal activation of the process [21]. The laser power dependence, shown in Fig. 5c) and **d)** also confirms TADF, as the intensity of fluorescence in the DF time region has a linear dependence on the excitation dose indicating that DF originates from a unimolecular process [22].

From the integrated areas of the DF and PF regions, we can calculate the DF to PF ratio, Φ_{DF}/Φ_{PF} [23]. This is a key parameter to estimate the contribution of TADF to the overall exciplex emission, and to determine the RISC rate. For the **TAPC:PBD**, exciplex, Φ_{DF}/Φ_{PF} was calculated to be 0.14 which suggests that the contribution of DF to the total emission is relatively small, fully consistent with the relatively large ST gap in the **TAPC:PBD** exciplex.

The reverse intersystem crossing rate can be estimated using **Equation (2)**, where ϕ_{RISC} is the yield of singlet states created by RISC, τ_{DF} is the delayed fluorescence lifetime, and $\int I_{DF}\,dt$ and $\int I_{PF}\,dt$ are the integrated areas of the delayed fluorescence and prompt fluorescence regions of the decay curve in Fig. 5a) [24–26].

$$k_{RISC} = \frac{\phi_{RISC}}{\tau_{DF}}\left(1 + \frac{\int I_{DF}\,dt}{\int I_{PF}\,dt}\right) \quad (2)$$

The RISC rate determined for the **TAPC:PBD** exciplex, $k_{RISC} = (6 \pm 4) \times 10^4 s^{-1}$, is much slower than the value reported previously [24,27]. However, this is fully consistent with the small TADF contribution to the overall exciplex emission and with the relatively large ΔE_{ST} in the **TAPC:PBD** exciplex.

The low amount of DF displayed by the exciplex system is also consistent with the measurements of the steady state emission spectra obtained as a function of temperature. Fig. 6 shows the emission spectra of the **TAPC:PBD** exciplex, in vacuum, obtained under 305 nm excitation in a range of temperatures, from 320K down to 80K. For materials where TADF dominates, the intensity of the overall emission is expected

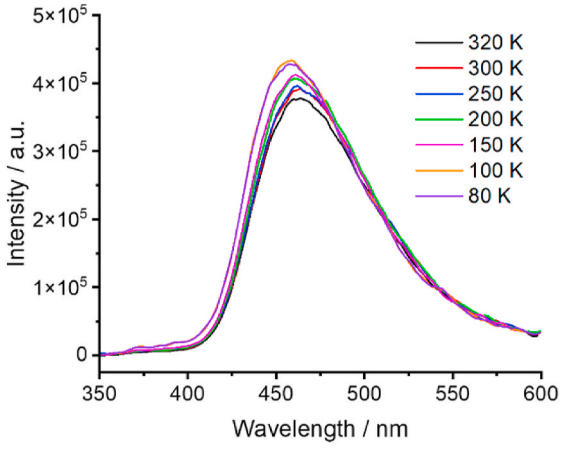

Fig. 6. Steady state emission of the **TAPC:PBD** exciplex obtained as a function of temperature, excited at 305 nm.

to increase with temperature. This is because the RISC rate increases exponentially with temperature, therefore, more singlets are formed at higher temperature as there is more thermal energy to overcome the singlet-triplet energy gap. This is demonstrated in Fig. 5b) for the DF component. However, when considering the overall emission, PF + DF, non-radiative processes are also facilitated at higher temperatures, which may reduce the overall amount of photoluminescence [28]. In the case of the **TAPC:PBD** exciplex, the non-radiative processes affecting both PF and DF seem to dominate, and the overall emission intensity decreases with increasing temperature, as illustrated in Fig. 6.

So far, we have characterized the **TAPC:PBD** exciplex, showing that this system is capable of harvesting triplet states, despite the slow RISC rate and weak PLQY.

2.2. *Exploring the FRET mechanism between the TAPC:PBD exciplex and TTPA*

Crucially, we will demonstrate in this section that most energy losses can be overcome by carefully choosing the terminal emitter in a hyperfluorescence blend. The key is that the energy transfer rate is sufficiently fast to rapidly move singlet and triplet states from the triplet harvesting unit to the emitter, therefore, suppressing non-radiative losses. In this section, a highly fluorescent dopant molecule, **TTPA**, is added to the **TAPC:PBD** exciplex to investigate the effect on PLQY and triplet harvesting efficiency.

The absorption and emission spectra of **TTPA** are given in Fig. 7a).

TTPA contains an absorption peak around 300 nm, which is close to the absorption of **PBD** and **TAPC**. This makes avoiding direct **TTPA** excitation difficult, and thus characterizing the hyperfluorescence mechanism more complex, as it is preferable that **TAPC** or **PBD** are first excited to form the exciplex, and triplet harvesting could occur prior to energy transfer. However, the extinction coefficient of **TTPA**, $(7.4 \pm 0.5) \times 10^3\ M^{-1}cm^{-1}$ at 355 nm, using concentrations in the range 0.88–7.0 μM, is much lower than that of **PBD,** which has $\varepsilon = (4.0 \pm 0.3) \times 10^4\ M^{-1}\ cm^{-1}$ at 355 nm. The extinction coefficient of **TTPA** as a function of wavelength is shown in Fig. 8. Moreover, the **TTPA** concentration is much lower than the concentration of **TAPC** or **PBD**. Therefore, even when **TTPA** is added to the blend, **PBD** will still be excited preferentially, and thus the exciplex will be formed before energy transfer occurs.

The absorption peak of **TTPA** at 460 nm is also noteworthy as it overlaps perfectly with the emission of the exciplex, shown in Fig. 9a). A large overlap between the two spectra is required for FRET to be efficient [29].

The emission of **TTPA** peaks at 547 nm with a full width at half maximum (FWHM) of 57.9 nm which is much narrower than the exciplex emission with a FWHM of 79.8 nm. The emission decay of **TTPA** (in 2 % Zeonex film) is given in Fig. 7b), showing a fluorescence lifetime of (18.2 ± 0.2) ns, calculated from a single exponential fit. A short fluorescence lifetime is desirable for the dopant as the fluorescence is fast enough to outcompete non-radiative loss mechanisms [30]. The PLQY of **TTPA** was measured in Zeonex films with 1 % and 2 % **TTPA** content, showing values of 0.90 and 0.87, respectively.

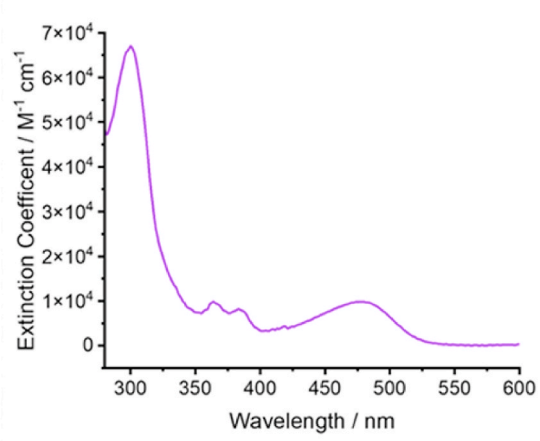

Fig. 8. Extinction coefficient of **TTPA** as a function of wavelength.

Fig. 9a) shows the absorption spectra of **TTPA** and emission of the **TAPC:PBD** exciplex showing excellent spectral overlap. Fig. 9b) shows the emission spectra of **TAPC:PBD** 1:1 films doped with different concentrations of **TTPA**. Even at low concentration, the emission mainly comes from **TTPA**, and only a residual exciplex emission is observed at low **TTPA** concentration. This demonstrates that FRET from the exciplex system to **TTPA** is very efficient. As concentration of **TTPA** increases, the amount of exciplex emission decreases, as expected. This is because, the average distance between exciplex and dopant species decreases causing an increase in the rate of FRET, k_{FRET}, which outcompetes the fluorescence rate from the exciplex. The emission slightly red shifts with increasing **TTPA** concentration. This is probably due to self-absorption caused by the small Stokes shift of **TTPA** or by some self-aggregation of **TTPA** molecules which can become more significant at higher concentration.

The concentration of **TTPA** was kept low to avoid Dexter triplet-triplet energy transfer between the triplet state of the exciplex and the triplet state of **TTPA**. Dexter transfer works as a potential loss mechanism, as excitons become trapped in the dark triplet state of **TTPA**, and no triplet harvesting is possible in this case. As the efficiency of the Dexter process varies exponentially with distance, by decreasing **TTPA** concentration, the Dexter transfer can be effectively suppressed [31].

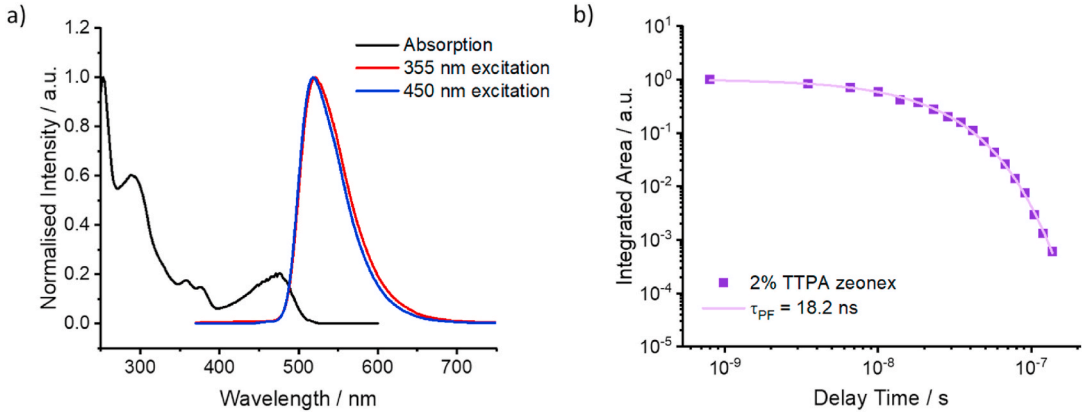

Fig. 7. a) **TTPA** absorption and emission spectra excited at both 355 and 450 nm. The spectra are obtained in a **TTPA**/Zeonex spin coated film with 2 % w/w dopant concentration. b) Fluorescence decay of **TTPA** obtained in Zeonex film, also with 2 % w/w dopant concentration. $\lambda_{ex} = 355$ nm.

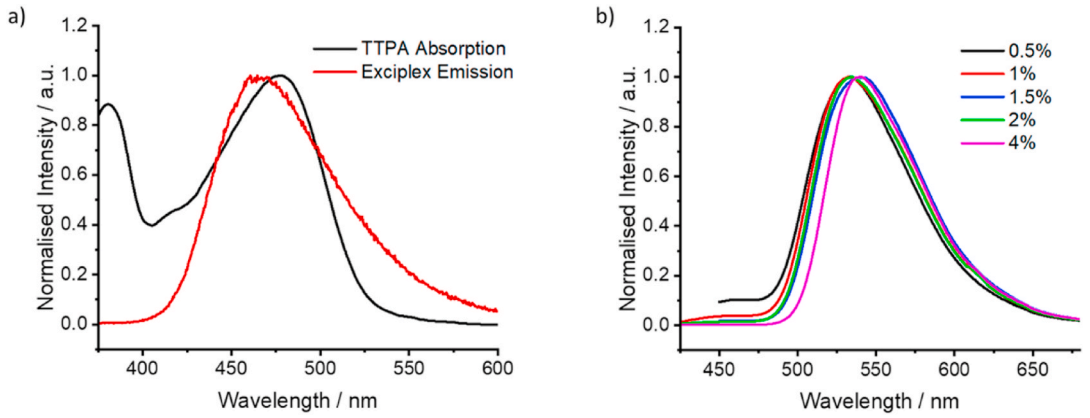

Fig. 9. a) Absorption spectra of **TTPA** and emission of the **TAPC:PBD** exciplex showing large overlap. b) Emission spectra of the **TAPC:PBD:TTPA** (50:50:x) blend obtained for different **TTPA** dopant concentrations. $\lambda_{ex} = 355$ nm.

However, FRET is operative over longer distances, and is thus largely not affected by using a low **TTPA** concentration [32].

The measured PLQY values in air for the doped exciplex system with different **TTPA** concentrations increases from 0.12 to 0.70 as the **TTPA** concentration increases, showing that as the energy transfer rate increases, other energy dissipation processes become less competitive. The PLQY is optimised at 2 % **TTPA** as this highest concentration has the shortest distance between host and dopant molecules.

Fig. 10a) shows the luminescence decay of the **TAPC:PBD:TTPA** (50:50:x) blend obtained as a function of **TTPA** concentration under 355 nm excitation. Increasing the concentration of **TTPA** clearly results in rapid decay of **TTPA** emission. However, the decay of **TTPA** luminescence is always longer than the decay of "isolated" **TTPA** fluorescence observed in Zeonex, giving clear indication that the triplet states of the **TAPC:PBD** exciplex are being harvested and contributing to the FRET process. Therefore, the RISC rate can outcompete the rate of triplet-triplet energy transfer between the exciplex and **TTPA**, thus avoiding this energy dissipation route. As the concentration of **TTPA** increases, FRET also becomes more efficient, making it possible that the FRET rate, k_{FRET}, becomes faster and competes with the intersystem crossing rate, k_{ISC}, in the **TAPC:PBD** exciplex, as already mentioned above. In this situation, less triplet states of the exciplex will be formed under optical excitation, hence resulting in weaker delayed fluorescence to be observed as the **TTPA** concentration increases. Also, as **TTPA** concentration increases, there is more chance for DET to occur which decreases the population of exciplex triplet states.

The DF/PF ratio can be calculated from the decay curves in Fig. 10a) at each **TTPA** doping concentration in the same way as DF/PF was calculated for the **TAPC:PBD** exciplex from Fig. 5a). The values are given in Table 3. As the concentration of **TTPA** increases, the Φ_{DF}/Φ_{PF} ratio decreases which indicates that FRET from the exciplex to **TTPA** is getting faster and competing with ISC in the exciplex. Since FRET is efficient, less triplet states are formed in the first place, therefore, we observe less triplet harvesting and hence less DF.

Fig. 11 shows the time resolved emission spectra measured at different delay times for the exciplex and **TTPA** doped films. Even at long delay times, the emission of the blend films comes clearly from **TTPA** (except in the **TAPC:PBD** blend with no **TTPA**), showing that FRET from the exciplex to the **TTPA** outperforms the radiative decay from the exciplex. However, as the concentration of **TTPA** increases, the delayed fluorescence decay becomes faster. Therefore, at longer delay times, the intensity of the emission decreases with a higher **TTPA** concentration.

Table 3
Key kinetic parameters for the **TAPC:PBD:TTPA** blend obtained as function of **TTPA** content.

	TAPC:PBD	0.5 % **TTPA**	1.5 % **TTPA**	2 % **TTPA**
PLQY/%	0.12	0.42	0.53	0.70
DF/PF ratio	0.14	0.13	0.10	0.06
τ_{PF}/ns	65.5	39.4	24.7	22.6
$k_{PF}/10^7$ s^{-1}	1.5	2.5	4.0	4.4
$k_{FRET}/10^7$ ns^{-1}	–	1.0	2.5	2.9
R_{DA}/nm	–	4.6	3.9	3.8
Φ_{FRET}/%	–	0.84	0.94	0.95

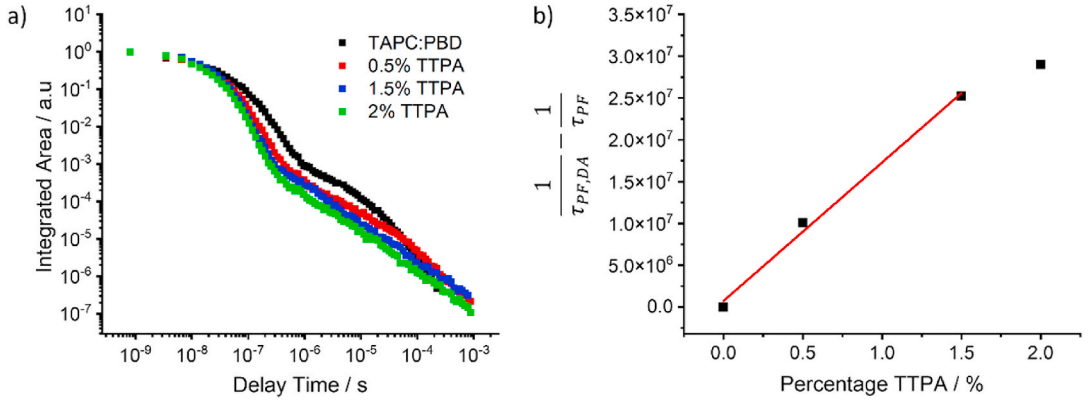

Fig. 10. a) Time resolved photoluminescence decay of **TAPC:PBD:TTPA** (50:50:x) blend as a function of **TTPA** concentration obtained with 355 nm excitation at room temperature. b) A plot of the difference between the reciprocal lifetimes with the fluorescent dopant, $\tau_{PF,DA}$, and without, τ_{PF} *vs* TTPA doping concentration as a w/w percentage.

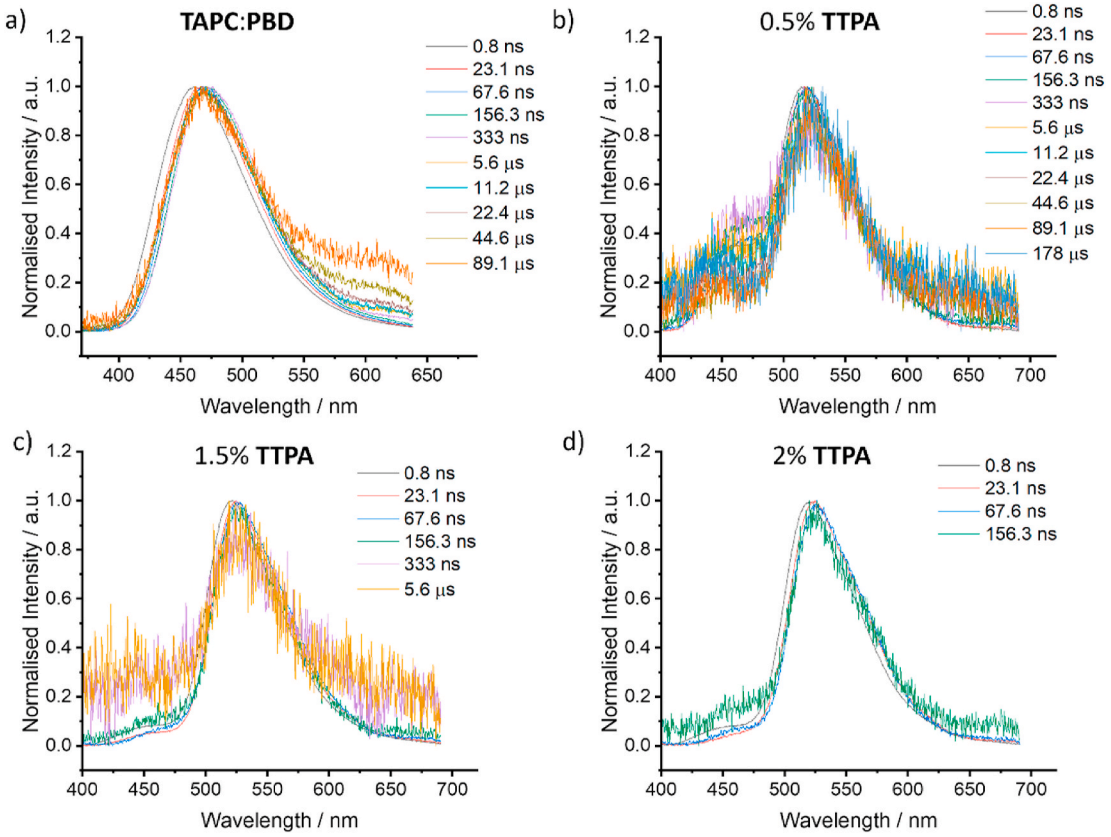

Fig. 11. Time resolved emission spectra measured at different delay times (shown in the legends) by excitation at 355 nm for a) **TAPC:PBD** 1:1 film, b), c) and d) for **TAPC:PBD** with 0.5 %, 1.5 % and 2 % **TTPA** doping concentration, respectively.

Finally, the energy level diagram describing the hyperfluorescence mechanism in the **TAPC:PBD:TTPA** blend is shown in Fig. 12, highlighting the different energy dissipation pathways. The **TAPC:PBD** exciplex is formed in the singlet state, S_1, as it is created under conservation of spin angular momentum by excitation of **PBD** to its first excited singlet state [33]. The exciplex S_1 can decay by fluorescing; undergoing non radiative decay or transition to the lowest excited triplet state by intersystem crossing; the rate constants for these processes are labelled k_r^S, k_{nr}^S and k_{ISC}, respectively. Due to the small energy gap between the singlet and triplet states in the exciplex, the triplet states can be upconverted back to the exciplex singlet state. This process has a rate constant labelled k_{RISC}. From the exciplex to **TTPA**, there are two possible energy transfer processes. One is a singlet-to-singlet transition known as Förster resonance energy transfer (FRET) which will transfer energy to the emissive S_1 state of **TTPA**. The rate of FRET is labelled k_{FRET}. The other possibility is Dexter energy transfer (DET) which is a triplet-to-triplet transition with rate constant k_{DET}. **TTPA** is not a triplet harvesting material so any energy transfer to its triplet state will cause energy loss.

An expression for the lifetime of the exciplex prompt fluorescence can be obtained by considering the decay mechanisms of the exciplex singlet state shown in Fig. 12. In the absence of dopant, we have an expression for the prompt fluorescence lifetime, $\tau_{PF,D}$, given by **Equation (3)**.

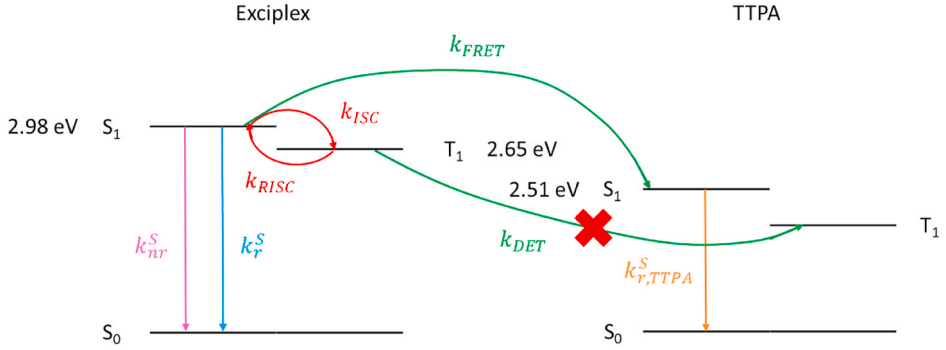

Fig. 12. Energy level diagram showing the photophysical processes involved in the system studied in this work. The energies of the exciplex and **TTPA** singlet, S_1, and triplet, T_1, states are given. The different processes are labelled by their rate constants. The exciplex singlet state can decay by fluorescence, k_r^S, non-radiative decay, k_{nr}^S, or intersystem crossing, k_{ISC}. Reverse intersystem crossing, k_{RISC} is possible from the exciplex T_1 to S_1 state. The two possible energy transfer pathways from the exciplex to **TTPA**, Förster resonance energy transfer, k_{FRET}, and Dexter energy transfer, k_{DET}, are shown. Upon formation of the **TTPA** S_1, the state can fluoresce to the ground state, S_0, with rate constant $k_{r,TTPA}^S$.

$$\tau_{PF,D} = \frac{1}{k_r^S + k_{nr}^S + k_{ISC}} \quad (3)$$

where k_r^S is the radiative decay rate of the singlet, k_{nr}^S is the rate of non-radiative decay of the singlet, and k_{ISC} is the rate of intersystem crossing to the triplet state.

In the presence of a dopant, there is an additional decay of the exciplex singlet state by Förster resonance energy transfer (FRET) as shown in Fig. 12. Therefore, the rate of FRET, k_{FRET}, is also included in the expression for the PF lifetime [34].

$$\tau_{PF,DA} = \frac{1}{k_r^S + k_{nr}^S + k_{ISC} + k_{FRET}[TTPA]} \quad (4)$$

This means that as the concentration of dopant is increased, the rate of FRET is also increasing as the process is more efficient when the distance is reduced and hence τ_{PF} decreases. This is shown in Fig. 10a) as the PF decay gets faster with increasing **TTPA** concentration and in Table 3 which gives the calculated τ_{PF} values showing a decrease with increasing **TTPA** concentration.

From equations (3) and (4), we can derive an expression for the FRET rate:

$$k_{FRET}[TTPA] = \frac{1}{\tau_{PF,DA}} - \frac{1}{\tau_{PF,D}} \quad (5)$$

Where $\tau_{PF,DA}$ and $\tau_{PF,D}$ are the prompt fluorescence lifetimes with and without the dopant, respectively. The k_{FRET} values obtained at different **TTPA** doping concentrations are given in Table 3. k_{PF} for the exciplex is $1.6 \times 10^7\ s^{-1}$, which comparing this to k_{FRET}, shows that FRET is much faster than fluorescence from the exciplex. This explains why little exciplex emission is observed in the blend with **TTPA**. Fig. 10b) shows the variation of $k_{FRET}[TTPA]$ with **TTPA** concentration. From **Equation (5)**, this variation is expected to be linear. This is obeyed strongly up to 1.5 % doping concentration. At higher concentration, the graph levels off showing that the energy transfer is already very efficient at 1.5 % and increasing the doping concentration further does not significantly increase the energy transfer efficiency and hence decrease the prompt fluorescence lifetime.

The Förster radius, R_0, can be defined as the intermolecular distance at which the FRET rate constant, k_{FRET}, is equal to the reciprocal of the fluorescence lifetime of the donor (in this case the exciplex). **Equation (6)** gives an expression for R_0:

$$R_0 = 0.2108 \left(\frac{\kappa^2 \Phi_D}{\eta^4} J\right)^{\frac{1}{6}} \quad (6)$$

Where κ^2 is taken to be 2/3 assuming that the dipole orientation is random, Φ_D is the PLQY of the host material, J is the overlap integral between the PL spectrum of the host and the extinction coefficient spectrum of the dopant, and η is the refractive index taken to be 1.4 [35,36]. From **Equation (6)**, the Förster radius was calculated to be $R_0 = 6.1$ nm. This is a large Förster radius due to the significant overlap between **TTPA** absorption and **TAPC:PBD** emission, which is consistent with the efficient FRET and explains why almost no exciplex emission is observed even at very low **TTPA** doping concentrations.

From the theory of FRET, k_{FRET} can also be expressed as:

$$k_{FRET} = \frac{\Phi_D}{\tau_{PF,D}} \left(\frac{R_0}{R_{DA}}\right)^{\frac{1}{6}} \quad (7)$$

Where R_{DA} is the intermolecular distance between the exciplex and the dopant [37–39]. The values of R_{DA} calculated from rearranging **Equation (7)** are given in Table 3. The results show that the average distance between exciplex and **TTPA** molecules is less than R_0 which facilitates efficient FRET.

The efficiency of FRET, Φ_{FRET}, is given by **Equation (8)** [31]:

$$\Phi_{FRET} = \frac{1}{1 + \left(\frac{R_{DA}}{R_0}\right)^6} \quad (8)$$

For the **TAPC:PBD** + **TTPA** system the Φ_{FRET} values given in Table 3 are very high and close to 1 showing efficient energy transfer from the exciplex singlet state to the singlet state of the dopant **TTPA**. Φ_{FRET} does not increase significantly between 1.5 and 2 % doping concentration which is consistent with the levelling off in Fig. 10b).

2.3. OLED devices

Prototype devices were fabricated with the structure: **ITO** | **HAT-CN** (5 nm) | **TAPC** (45 nm) | **TAPC:PBD** 50:50 co 1 % **TTPA** (30 nm) | **TPBi** (50 nm) | **LiF** (0.8 nm) | **Al** (70 nm). **ITO** and **LiF/Al** are used as the anode and cathode, respectively. **HAT-CN** serves as the hole injection layer, while **TAPC** and **TPBi** are employed as hole-transport and electron-transport layers, respectively.

The devices show stable green emission with the electroluminescence (EL) consistent with the photoluminescence of **TTPA**, peaking at 525 nm (Fig. 13a)). The FWHM of the spectra is 67.1 nm which is similar to that observed for the photoluminescence of the **TAPC:PBD** + 2 % **TTPA** film. There are two small peaks in the EL at approximately at 400 and 450 nm. They can be assigned to **TPBi** emission at around 400 nm and the emission of **TAPC:PBD** exciplex for the shoulder around 450 nm.

This device structure gives a maximum external quantum efficiency (EQE) of 2.2 % and maximum current efficiency (CE) of 7.3 cd A^{-1}. Fig. 13b) shows the EQEs as a function of current density which demonstrates a pronounced efficiency roll-off. Fig. 13c) shows the luminescence-voltage-current density curves for the devices. From here the turn-on voltage is calculated to be 3 V at a luminance of 1 cd m^{-2}. While the causes for the low EQE of the device and pronounced roll-off may appear from different sources, analysing these results is very useful to promote understanding of differences arising from optical *vs* electrical excitations. Under optical excitation only singlet states are initially created, and the delayed fluorescence originates from triplets initially formed by ISC in the exciplex, which can up-convert to the singlet state *via* a relatively slow RISC process ($10^4\ s^{-1}$). The fact that delayed **TTPA** fluorescence is observed indicates that the ISC rate within the exciplex can compete with the fast FRET rate to **TTPA**. However, the number of triplets formed must be relatively small, compared with the 75 % triplets formed under electrical excitation. Due to the relatively slow RISC, a significant fraction of this pool of triplet states created by electrical excitation is likely to become trapped and be susceptible to suffer polaron quenching, which may explain the poor performance of the devices. Therefore, while a fast FRET rate is key to avoid energy losses, and a high luminescence efficiency can be achieved under optical excitation by fine tuning of the energy transfer rate, a fast RISC rate is still necessary to minimize EL quenching in devices caused by be the interaction of trapped triplets and polarons. The low EQE of the device could be due to excitons becoming trapped in the triplet state of **PBD**. It has been reported that the triplet energy of the exciplex being lower than the exciplex components is important [40].

3. Conclusion

In conclusion an in-depth study of an exciplex system using **TAPC** as an electron donor and **PBD** as an electron acceptor has been carried out. The exciplex demonstrated a relatively low PLQY and slow triplet harvesting rate. We have addressed the previously overestimated k_{RISC} for the exciplex. The overestimate arose because the time resolved measurements were not taken out to a long enough time range. Taking our measurements to the ms time range, we were able to observe the whole DF region and obtain a DF lifetime which is consistent with the large S-T gap and small DF/PF ratio. However, when doped with a bright

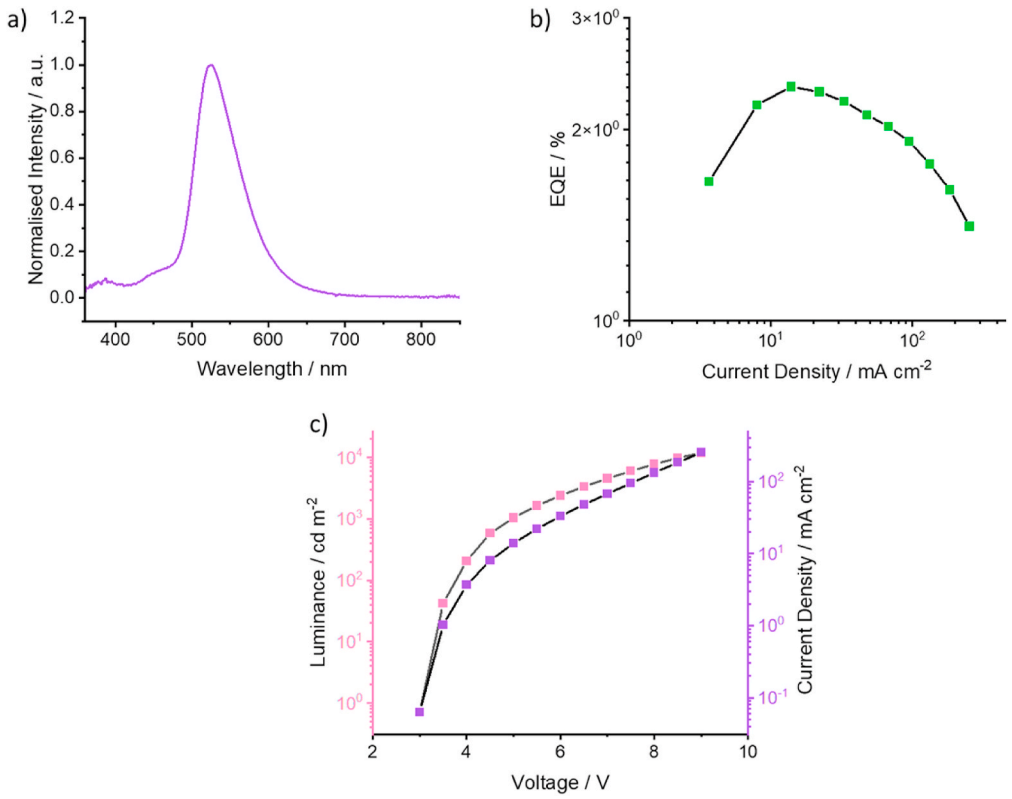

Fig. 13. Electrical and electroluminescent properties of the fabricated device: a) Electroluminescence, b) External quantum efficiency (EQE) as a function of current density and c) Luminescence-voltage- current density curve for the fabricated devices.

fluorescent guest, **TTPA**, the rapid energy transfer is able to facilitate a very high PLQY and outcompete energy loss mechanisms such as non-radiative decay. We have shown the power of hyperfluorescence to enhance light output.

3.1. Experimental section

The UV–vis absorption data was recorded using a Shimadzu Spectrophotometer UV-3600. Emission spectra were collected on a Horiba Fluorolog spectrometer with a Xe lamp excitation source. Time resolved photoluminescence was collected using the third harmonic of a pulsed Nd:YAG laser (355 nm) or a N_2 laser (337 nm). The emission is detected on a gated iCCD camera (Stanford Computer Optics) with a sub-nanosecond resolution. Temperature dependence measurements were taken using a Janis Research liquid nitrogen cryostat VNF-100. Photoluminescence quantum yields were recorded using a Hamamatsu Quantaurus-QY system.

OLED devices were fabricated on indium tin oxide (**ITO**) coated glass substrates with a sheet resistance of 20 Ω/sq and **ITO** thickness of 100 nm. Prior to evaporation, the substrates were washed with distilled water then acetone followed by sonication in acetone and isopropanol, for 15 min each. Substrates were dried with compressed air and placed into an oxygen plasma generator for 6 min. Layers were thermally deposited using a Kurt J. Lesker Spectros II deposition system at a pressure of 10^{-6} mbar. The layers were evaporated at rates between 0.1 and 2.5 Å s^{-1} depending on the thickness of the layer. The devices produced had pixel areas of 4 × 4, 4 × 2 or 2 × 2 mm. The characterisation of devices was done using a 10-inch integrating sphere (Labsphere) connected to a Source Measure Unit (SMU, Keithley) and a spectrometer USB4000.

CRediT authorship contribution statement

Lucy A. Weatherill: Writing – review & editing, Writing – original draft, Visualization, Investigation, Formal analysis. **Ross Milverton:** Investigation. **Piotr Pander:** Writing – review & editing, Validation, Investigation. **Fernando B. Dias:** Writing – review & editing, Writing – original draft, Validation, Supervision, Resources, Project administration, Methodology, Investigation, Conceptualization.

Declaration of competing interest

The authors declare that they have no known competing financial interests or personal relationships that could have appeared to influence the work reported in this paper.

Data availability

Data will be made available on request.

References

[1] H. Uoyama, K. Goushi, K. Shizu, H. Nomura, C. Adachi, Highly efficient organic light-emitting diodes from delayed fluorescence, Nature 492 (2012) 234–238, https://doi.org/10.1038/nature11687.
[2] M. Colella, P. Pander, D.D.S. Pereira, A.P. Monkman, Interfacial TADF exciplex as a tool to localize excitons, improve efficiency, and increase OLED lifetime, ACS Appl. Mater. Interfaces 10 (2018) 40001–40007, https://doi.org/10.1021/acsami.8b15942.
[3] P.L. Santos, J.S. Ward, P. Data, A.S. Batsanov, M.R. Bryce, F.B. Dias, A. P. Monkman, Engineering the singlet-triplet energy splitting in a TADF molecule, J Mater Chem C Mater 4 (2016) 3815–3824, https://doi.org/10.1039/c5tc03849a.
[4] Y. Im, M. Kim, Y.J. Cho, J.A. Seo, K.S. Yook, J.Y. Lee, Molecular design strategy of organic thermally activated delayed fluorescence emitters, Chem. Mater. 29 (2017) 1946–1963, https://doi.org/10.1021/acs.chemmater.6b05324.
[5] F.B. Dias, T.J. Penfold, A.P. Monkman, Photophysics of thermally activated delayed fluorescence molecules, Methods Appl. Fluoresc. 5 (2017), https://doi.org/10.1088/2050-6120/aa537e.

[6] H.B. Kim, J.J. Kim, Recent progress on exciplex-emitting OLEDs, Journal of Information Display 20 (2019) 105–121, https://doi.org/10.1080/15980316.2019.1650838.
[7] K. Goushi, K. Yoshida, K. Sato, C. Adachi, Organic light-emitting diodes employing efficient reverse intersystem crossing for triplet-to-singlet state conversion, Nat. Photonics 6 (2012) 253–258, https://doi.org/10.1038/nphoton.2012.31.
[8] D. Graves, V. Jankus, F.B. Dias, A. Monkman, Photophysical investigation of the thermally activated delayed emission from films of m-MTDATA:PBD exciplex, Adv. Funct. Mater. 24 (2014) 2343–2351, https://doi.org/10.1002/adfm.201303389.
[9] H. Tanaka, K. Shizu, H. Miyazaki, C. Adachi, Efficient green thermally activated delayed fluorescence (TADF) from a phenoxazine–triphenyltriazine (PXZ–TRZ) derivative, Chem. Commun. 48 (2012) 11392–11394, https://doi.org/10.1039/c2cc36237f.
[10] X. Song, D. Zhang, H. Li, M. Cai, T. Huang, L. Duan, Exciplex system with increased donor-acceptor distance as the sensitizing host for conventional fluorescent OLEDs with high efficiency and extremely low roll-off, ACS Appl. Mater. Interfaces 11 (2019) 22595–22602, https://doi.org/10.1021/acsami.9b05963.
[11] T. Komino, H. Nomura, T. Koyanagi, C. Adachi, Suppression of efficiency roll-off characteristics in thermally activated delayed fluorescence based organic light-emitting diodes using randomly oriented host molecules, Chem. Mater. 25 (2013) 3038–3047, https://doi.org/10.1021/cm4011597.
[12] Latt. Nat. 750 (2000). www.nature.com.
[13] H. Lee, R. Braveenth, S. Muruganantham, C.Y. Jeon, H.S. Lee, J.H. Kwon, Efficient pure blue hyperfluorescence devices utilizing quadrupolar donor-acceptor-donor type of thermally activated delayed fluorescence sensitizers, Nat. Commun. 14 (2023), https://doi.org/10.1038/s41467-023-35926-1.
[14] D.L. Dexter, A theory of sensitized luminescence in solids, J. Chem. Phys. 21 (1953) 836–850, https://doi.org/10.1063/1.1699044.
[15] P. Wei, D. Zhang, L. Duan, Modulation of förster and dexter interactions in single-emissive-layer all-fluorescent WOLEDs for improved efficiency and extended lifetime, Adv. Funct. Mater. 30 (2020), https://doi.org/10.1002/adfm.201907083.
[16] H. Du, Q. Zhou, Y. Yu, C. Liu, J. Li, C. Zhang, Z. Ji, Z. Pang, High-PLQY and efficient upconverted fluorescence of the TAPC/PBD exciplex with fluorescent guests, J. Phys. Chem. C 126 (2022) 11229–11237, https://doi.org/10.1021/acs.jpcc.2c02993.
[17] B.S. Kim, J.Y. Lee, Engineering of mixed host for high external quantum efficiency above 25% in green thermally activated delayed fluorescence device, Adv. Funct. Mater. 24 (2014) 3970–3977, https://doi.org/10.1002/adfm.201303730.
[18] Y. Wang, F. Teng, C. Ma, Z. Xu, Y. Hou, S. Yang, Y. Wang, X. Xu, Green to white to blue OLEDs by using PBD as a chromaticity-tuning layer, Displays 25 (2004) 237–239, https://doi.org/10.1016/j.displa.2004.09.016.
[19] T. Higuchi, H. Nakanotani, C. Adachi, High-efficiency white organic light-emitting diodes based on a blue thermally activated delayed fluorescent emitter combined with green and red fluorescent emitters, Adv. Mater. 27 (2015) 2019–2023, https://doi.org/10.1002/adma.201404967.
[20] J.H. Lee, S.H. Cheng, S.J. Yoo, H. Shin, J.H. Chang, C.I. Wu, K.T. Wong, J.J. Kim, An exciplex forming host for highly efficient blue organic light emitting diodes with low driving voltage, Adv. Funct. Mater. 25 (2015) 361–366, https://doi.org/10.1002/adfm.201402707.
[21] R.S. Nobuyasu, Z. Ren, G.C. Griffiths, A.S. Batsanov, P. Data, S. Yan, A. P. Monkman, M.R. Bryce, F.B. Dias, Rational design of TADF polymers using a donor-acceptor monomer with enhanced TADF efficiency induced by the energy alignment of charge transfer and local triplet excited states, Adv. Opt. Mater. 4 (2016) 597–607, https://doi.org/10.1002/adom.201500689.
[22] F.B. Dias, Kinetics of thermal-assisted delayed fluorescence in blue organic emitters with large singlet-triplet energy gap, Phil. Trans. Math. Phys. Eng. Sci. 373 (2015), https://doi.org/10.1098/rsta.2014.0447.
[23] C. Grewer, H.-D. Brauer, Mechanism of the triplet-state quenching by molecular oxygen in solution. https://pubs.acs.org/sharingguidelines, 1994.
[24] M. Chapran, P. Pander, M. Vasylieva, G. Wiosna-Salyga, J. Ulanski, F.B. Dias, P. Data, Realizing 20% external quantum efficiency in electroluminescence with efficient thermally activated delayed fluorescence from an exciplex, ACS Appl. Mater. Interfaces 11 (2019) 13460–13471, https://doi.org/10.1021/acsami.8b18284.
[25] H.F. Higginbotham, C.L. Yi, A.P. Monkman, K.T. Wong, Effects of ortho-phenyl substitution on the rISC rate of D-A type TADF molecules, J. Phys. Chem. C 122 (2018) 7627–7634, https://doi.org/10.1021/acs.jpcc.8b01579.
[26] P.L. Dos Santos, F.B. Dias, A.P. Monkman, Investigation of the mechanisms giving rise to TADF in exciplex states, J. Phys. Chem. C 120 (2016) 18259–18267, https://doi.org/10.1021/acs.jpcc.6b05198.
[27] D. Berenis, G. Kreiza, S. Juršėnas, E. Kamarauskas, V. Ruibys, O. Bobrovas, P. Adomėnas, K. Kazlauskas, Different RISC rates in benzoylpyridine-based TADF compounds and their implications for solution-processed OLEDs, Dyes Pigments 182 (2020), https://doi.org/10.1016/j.dyepig.2020.108579.
[28] J.P. Claude, T.J. Meyer, Temperature dependence of nonradiative decay. https://pubs.acs.org/sharingguidelines, 1995.
[29] K. Stavrou, L.G. Franca, A. Danos, A.P. Monkman, Key requirements for ultraefficient sensitization in hyperfluorescence organic light-emitting diodes, Nat. Photonics 18 (2024) 554–561, https://doi.org/10.1038/s41566-024-01395-1.
[30] S.J. Wu, X.F. Fu, D.H. Zhang, Y.F. Sun, X. Lu, F.L. Lin, L. Meng, X.L. Chen, C.Z. Lu, Thermally activated delayed fluorescence with nanosecond emission lifetimes and minor concentration quenching: achieving high-performance nondoped and doped blue OLEDs, Adv. Mater. 36 (2024), https://doi.org/10.1002/adma.202401724.
[31] A. Cravcenco, C. Ye, J. Gräfenstein, K. Börjesson, Interplay between förster and dexter energy transfer rates in isomeric donor-bridge-acceptor systems, J. Phys. Chem. A 124 (2020) 7219–7227, https://doi.org/10.1021/acs.jpca.0c05035.
[32] J. Lakowicz, Principles of Fluorescence Spectroscopy, Springer US, Boston, MA, 2006, https://doi.org/10.1007/978-0-387-46312-4.
[33] M. Gordon, W.R. Ware, The Exciplex, Academic Press Inc., 1975.
[34] Y. Tang, Y. Liu, W. Ning, L. Zhan, J. Ding, M. Yu, H. Liu, Y. Gao, G. Xie, C. Yang, Manipulating Förster and Dexter interactions between a thermally activated delayed fluorescence host and a phosphorescent dopant for highly efficient solution-processed red and white OLEDs, J Mater Chem C Mater 10 (2022) 4637–4645, https://doi.org/10.1039/d1tc05470h.
[35] H. Sahoo, Förster resonance energy transfer - a spectroscopic nanoruler: principle and applications, J. Photochem. Photobiol. C Photochem. Rev. 12 (2011) 20–30, https://doi.org/10.1016/j.jphotochemrev.2011.05.001.
[36] A. Shoustikov, Y. You, P.E. Burrows, M.E. Thompson, S.R. Forrest, Orange and Red Organic Light-Emitting Devices Using Aluminum Tris (Shydroxyquinoxaline), 1997.
[37] T.H. Forster, 0TH Spiers Memorial Lecture Transfer Mechanisms of Electronic Excitation, n.d.
[38] H. Fukagawa, T. Shimizu, Y. Iwasaki, T. Yamamoto, Operational lifetimes of organic light-emitting diodes dominated by Förster resonance energy transfer, Sci. Rep. 7 (2017), https://doi.org/10.1038/s41598-017-02033-3.
[39] N.J. Turro, Modern Molecular Photochemistry, University Science Books, 1991.
[40] Y. Miao, G. Wang, M. Yin, Y. Guo, B. Zhao, H. Wang, Phosphorescent ultrathin emitting layers sensitized by TADF interfacial exciplex enables simple and efficient monochrome/white organic light-emitting diodes, Chem. Eng. J. 461 (2023), https://doi.org/10.1016/j.cej.2023.141921.